

Unitarity Constraints on Anomalous Top Quark Couplings to Weak Gauge Bosons

M. Hosch, K. Whisnant, and Bing-Lin Young

Department of Physics and Astronomy, Iowa State University, Ames, IA 50011, USA

Abstract

If there is new physics associated with the top quark, it could show up as anomalous couplings of the top quark to weak gauge bosons, such as $Zt\bar{t}$ and $Wt\bar{b}$ vector and axial-vector couplings. We use the processes $t\bar{t} \rightarrow Z^0 Z^0$, $t\bar{t} \rightarrow W^+ W^-$, and $t\bar{t} \rightarrow Z^0 H$ to obtain the unitarity constraints on these anomalous couplings, and combine these constraints with those from precision electroweak data. The unitarity constraints can impose additional limits on the anomalous couplings when the scale of new physics is as low as 2 TeV. A nonzero measurement of such an anomalous coupling leads to an upper limit on the new physics scale from the unitarity condition.

The combined CDF [1] and D0 [2] measurements give a top mass of $m_t = 175 \pm 9$ GeV. The large size of the top quark mass, near the scale of electroweak symmetry breaking, suggests that the interactions of the top quark may provide clues to the physics of electroweak symmetry breaking and possibly evidence for physics beyond the standard model.

If the new physics occurs above the electroweak symmetry breaking scale, its effects can be expressed as non-standard terms in an effective Lagrangian describing the physics at or below the new physics scale. Such non-standard interactions, in the form of anomalous vector and axial-vector couplings of the top quark to the W and Z bosons, will affect Z decay widths. The recent measurement of R_b [3], the ratio of the decay widths $Z \rightarrow b\bar{b}$ and $Z \rightarrow \text{hadrons}$, provides a motivation for studying these anomalous couplings [4,5]. Limits on these couplings from precision measurements at LEP and SLC have been obtained at the one-loop level [6].

In the standard model, the gauge symmetry enforces perturbative unitarity at all scales. In an effective theory with anomalous couplings the gauge symmetry is explicitly broken, the renormalizability is spoiled, and partial wave unitarity will be violated at high energies [7]. When such anomalous couplings are present in the effective interaction, a renormalizable Lagrangian containing the new physics should replace the effective Lagrangian at a scale Λ which is below the scale where unitarity is violated, so that perturbative unitarity is restored. Such unitarity constraints have been used recently to put limits on anomalous Yukawa couplings of the top quark [8] and on the couplings of higher dimension operators not accessible to existing accelerators [9].

In this paper we will examine the unitarity constraints on anomalous vector and axial vector couplings of the top quark to the W and Z by calculating the amplitudes for the processes $t\bar{t} \rightarrow t\bar{t}$, $t\bar{t} \rightarrow Z_L^0 Z_L^0$, $t\bar{t} \rightarrow W_L^+ W_L^-$, and $t\bar{t} \rightarrow Z_L^0 H$, where the L subscript refers to the longitudinal component. We parametrize the anomalous contributions to the $t\bar{t}Z$ and the tbW couplings as [4,6]

$$\delta\mathcal{L}_{eff} = \frac{-ig_2}{2\cos\theta} \bar{t}\gamma^\mu \left[\kappa_L^{NC}(1 - \gamma_5) + \kappa_R^{NC}(1 + \gamma_5) \right] tZ_\mu$$

$$-\frac{ig_2}{2\sqrt{2}}\left[\bar{t}\gamma^\mu(\kappa_L^{CC}(1-\gamma_5)+\kappa_R^{CC}(1+\gamma_5))bW_\mu^++h.c.\right], \quad (1)$$

where the κ 's are dimensionless parameters which are absent in the standard model.

The anomalous effective Lagrangian in Eq. 1 is the simplest possible modification of the weak sector which obeys certain elementary constraints. It contains only dimension 4 operators, and includes only standard neutral-current couplings for the b quark at tree level. This latter requirement arises from the experimental fact that the b -quark couplings to the Z are quite close to their Standard Model values. We do not include any extra sources of CP violation, so that the κ 's must be real. We do not include nonstandard photon couplings, so that electrodynamics is unaltered. Finally, we note that because we have not included all possible anomalous couplings, but rely upon the assumption that contributions from different couplings do not cancel each other, the results obtained here are not absolute predictions.

The anomalous coupling parameters in Eq. 1 will affect the interpretation of the electroweak measurements at LEP and SLC. In Ref. [6] the authors place restrictions on the anomalous coupling parameters using complete expressions for electroweak measurables which even include terms which are not enhanced by M_t^2/M_W^2 . In order to see the effect of the unitarity constraints, we will first update the limits with a recent analysis of the precision electroweak data [10], supplemented by the latest measurements of $R_b = \Gamma(b\bar{b})/\Gamma(\text{hadrons})$ [3], and include terms quadratic in the κ 's ignored in earlier analyses. We find that these seemingly small quadratic terms have a significant effect on the allowed regions in some cases. Then we will combine these results with constraints from unitarity. We find that the unitarity constraints can place additional limits on the anomalous couplings when the scale of new physics is as low as 2 TeV. Furthermore, since the data is not consistent with the Standard Model at the 90% CL, unitarity constraints place an upper limit on the scale of new physics represented by the κ 's in Eq. 1.

New physics at LEP and SLC can be parametrized in terms of the four parameters S , T , U [11] and $\delta_{b\bar{b}}$ [10,12] defined by $\Gamma(b\bar{b}) = \Gamma(b\bar{b})_{SM}(1 + \delta_{b\bar{b}})$, which can be expressed in

terms of R_b as $\delta_{b\bar{b}} = (R_b/R_b^{SM} - 1)/(1 - R_b)$. The anomalous coupling contributions to these variables (not counting the effects of a standard model top quark and Higg boson) are [6]

$$S = \frac{2}{3\pi} \left[2\kappa_R^{NC} - \kappa_L^{NC} - 3(\kappa_L^{NC})^2 - 3(\kappa_R^{NC})^2 \right] \log \frac{\mu^2}{M_Z^2}, \quad (2)$$

$$T = \frac{3}{8\pi s_Z^2} \frac{M_t^2}{M_W^2} \left[2\kappa_L^{CC} + 4\kappa_R^{NC} - 4\kappa_L^{NC} + (\kappa_L^{CC})^2 + (\kappa_R^{CC})^2 - 4(\kappa_L^{NC} - \kappa_R^{NC})^2 \right] \log \frac{\mu^2}{M_Z^2}, \quad (3)$$

$$U = \frac{1}{\pi} \left[-2\kappa_L^{CC} + 2\kappa_L^{NC} - (\kappa_L^{CC})^2 - (\kappa_R^{CC})^2 + 2(\kappa_L^{NC})^2 + 2(\kappa_R^{NC})^2 \right] \log \frac{\mu^2}{M_Z^2}, \quad (4)$$

$$\begin{aligned} \delta_{b\bar{b}} = & \frac{\alpha}{9\pi} \frac{1}{(8 - 12s_Z^2 + 9s_Z^4)} \frac{27s_Z^2}{8(1 - s_Z^2)} \frac{M_t^2}{M_W^2} \log \frac{\mu^2}{M_Z^2} \\ & \times \left[(4s_Z^4 - 18s_Z^2 + 9) (2\kappa_L^{CC} + (\kappa_L^{CC})^2 - 4(\kappa_R^{NC} - \kappa_L^{NC})^2) \right. \\ & \left. + 4(4s_Z^4 + 2s_Z^2 - 3)\kappa_L^{NC} + 2(4s_Z^4 - 28s_Z^2 + 15)\kappa_R^{NC} - (28s_Z^4 + 2s_Z^2 - 9)(\kappa_R^{CC})^2 \right], \quad (5) \end{aligned}$$

where μ is the renormalization scale and $s_Z^2 = \sin^2 \theta_W(M_Z)$. We keep the terms quadratic in the κ 's in our analysis, as they will affect the result even when the κ 's are not large. As in Ref. [6], we choose the scale $\mu = 2m_t$, which assumes that the new physics is related to the top quark mass, and take $m_t = 175$ GeV and $s_Z^2 = 0.2311$. We have also investigated the case $\mu = m_t$ and will comment on it later.

Recent data from LEP and SLC imply the following constraints due to new physics contributions [3,10]

$$S = -0.28 \pm 0.19_{-0.17}^{+0.08} \quad (6)$$

$$T = -0.20 \pm 0.26_{-0.12}^{+0.17} \quad (7)$$

$$U = -0.31 \pm 0.54 \quad (8)$$

$$\delta_{b\bar{b}} = 0.0130 \pm 0.0067, \quad (9)$$

where the second error in S and T is from varying M_H , the standard model Higgs mass, between 60 GeV (the lower value) and 1 TeV (the upper value), with a central value at 300 GeV. In all of our calculations we take $M_H = 300$ GeV. The values for the S , T and U parameters are taken from a recent global fit [10], and $\delta_{b\bar{b}}$ is the latest world average [3]. The error in $\delta_{b\bar{b}}$ includes the theoretical error in the Standard Model value of R_b , added in quadrature with the experimental error.

The CLEO measurement of $b \rightarrow s\gamma$ [13] also puts a constraint on κ_R^{CC} [14]. We have updated this limit using the most recent experimental data on m_t and $b \rightarrow s\gamma$ to get

$$-0.03 < \kappa_R^{CC} < 0.00. \quad (10)$$

We note that κ_R^{CC} is constrained to be very small and enters into Eqs. 2-5 only quadratically. As will be demonstrated later, the unitarity constraints also depend on κ_R^{CC} only quadratically, so that we will be able to consistently ignore its effects.

The constraints on the κ 's due to the precision electroweak data are most easily seen by looking at the allowed regions when two of the parameters are varied simultaneously. Figures 1a and 1b show the 90% CL bounds on κ_L^{NC} versus κ_R^{NC} and κ_L^{CC} versus κ_R^{NC} , respectively, where the other parameters are set to zero in each case, and we have set the renormalization scale at $\mu = 2m_t$. The region allowed by all the data is denoted by bold lines. As is evident from the figures, the most important constraints on the allowed regions are from the limits on T and $\delta_{b\bar{b}}$, although a further deviation from zero of the S parameter would have a significant effect on the allowed regions. The results of a three-parameter fit are shown in Fig. 2, where allowed regions of κ_L^{NC} versus κ_R^{NC} are shown for various values of κ_L^{CC} .

A brief remark on the importance of the terms quadratic in the κ 's in Eqs. 2-5 is in order. If the quadratic terms were not included, the allowed region in Fig. 1a would be reduced by roughly 90% in Fig. 1a, and the allowed region in Fig. 1b is nearly unaffected. Thus including the quadratic terms can be very important in determining the proper allowed region even when the magnitudes of the κ 's are less than unity. Furthermore, there is another allowed region in the case of Fig. 1b which is a reflection of the curves shown about $\kappa_L^{CC} = -1$. This extra solution, which requires the inclusion of the quadratic terms, simply changes the sign of the $Wt\bar{b}$ coupling from its standard model value.

In the calculation of the unitarity constraints, we initially consider the tree-level processes $t\bar{t} \rightarrow t\bar{t}$, $t\bar{t} \rightarrow Z_L Z_L$, $t\bar{t} \rightarrow W_L^+ W_L^-$, and $t\bar{t} \rightarrow Z_L H$, which will be affected by the anomalous couplings of Eq. 1. For each reaction we consider all helicity combinations for the t and \bar{t} . The

reactions with transverse vector bosons may be ignored since their rates are suppressed in comparison with the processes involving longitudinal vector bosons. We are most concerned with amplitudes that grow with increasing center of mass energy, \sqrt{s} , as they are guaranteed to violate unitarity at some scale. This consideration leads us to discard the processes $t\bar{t} \rightarrow t\bar{t}$ and $t\bar{t} \rightarrow Z_L H$, as they do not grow with \sqrt{s} , even with nonzero anomalous couplings. For the same reason, by considering separately each possible combination of the top quark and the antitop quark helicity, we are led to discard the processes $t_+ \bar{t}_- \rightarrow Z_L Z_L$, and $t_+ \bar{t}_- \rightarrow Z_L Z_L$. This leaves four independent processes which grow with \sqrt{s} . These four processes are sufficient to constrain the anomalous couplings in our model.

For the process $t\bar{t} \rightarrow Z_L Z_L$, the diagrams which contribute are the t - and u -channel exchange of a virtual top quark and the s -channel Higgs exchange. To leading order in s the helicity amplitudes are

$$T_{++}(t\bar{t} \rightarrow Z_L Z_L) = -T_{--}(t\bar{t} \rightarrow Z_L Z_L) = i\sqrt{2}G_f m_t \sqrt{s}[(1 + \kappa_L^{NC} - \kappa_R^{NC})^2 - 1]. \quad (11)$$

For the process $t\bar{t} \rightarrow W_L^+ W_L^-$ the diagrams which contribute are the t -channel exchange of a virtual b quark, and the s -channel exchange of the Z boson, Higgs boson, and photon. After retaining only leading terms proportional to s and \sqrt{s} , the helicity amplitudes are

$$\begin{aligned} T_{++}(t\bar{t} \rightarrow W_L^+ W_L^-) &= -T_{--}(t\bar{t} \rightarrow W_L^+ W_L^-) \\ &= i\sqrt{2}G_f m_t \sqrt{s}[(\kappa_L^{CC})^2 + 2\kappa_L^{CC} + (\kappa_R^{CC})^2 \\ &\quad + \cos(\theta)((\kappa_L^{CC})^2 + 2\kappa_L^{CC} + (\kappa_R^{CC})^2 - \kappa_L^{NC} - \kappa_R^{NC})] \end{aligned} \quad (12)$$

$$T_{+-}(t\bar{t} \rightarrow W_L^+ W_L^-) = i\sqrt{2}G_f s \sin(\theta)[(\kappa_R^{CC})^2 - \kappa_R^{NC}] \quad (13)$$

$$T_{-+}(t\bar{t} \rightarrow W_L^+ W_L^-) = i\sqrt{2}G_f s \sin(\theta)[(\kappa_L^{CC})^2 + 2\kappa_L^{CC} - \kappa_L^{NC}]. \quad (14)$$

As stated earlier, κ_R^{CC} appears only quadratically in the unitarity conditions (as was the case for its contributions to S , T , U , and δ_{bb}), so that its effects can be safely ignored in view of the constraint in Eq. 10. Henceforth, in all of our calculations we take $\kappa_R^{CC} = 0$.

With these expressions for the amplitudes, we may determine the constraints from partial wave unitarity. The J th partial wave amplitude for a process with helicity amplitude T is

$$a_{m,m'}^J = \frac{1}{32\pi} \int_{-1}^1 d(\cos \theta) d_{m,m'}^J(\theta) T_{m,m'}, \quad (15)$$

where $d_{m,m'}^J(\theta)$ is the Wigner d -function. For the channels we are considering, $m = 1$ for $t_+\bar{t}_-$, $m = 0$ for $t_+\bar{t}_+$, $t_-\bar{t}_-$, $W_L^+W_L^-$ and $Z_L Z_L$, and $m = -1$ for $t_-\bar{t}_+$ (likewise for m') [15]. Partial wave unitarity implies that $|a_{m,m'}^J| < 1$ for each amplitude listed in Eqs. 11-14. However, the most restrictive bound comes from eigenvalues of the coupled channel matrix for each value of J , each of which must also be less than 1. We consider only the $J = 0$ and $J = 1$ partial waves, as they give the strongest constraints. If we write the channels in the order $t_+\bar{t}_+$, $t_-\bar{t}_-$, $W_L^+W_L^-$, and $Z_L Z_L$ then the coupled channel matrix for the color singlet $J = 0$ partial wave is

$$a^0 = \frac{\sqrt{6}G_F}{16\pi}s \begin{pmatrix} 0 & 0 & T_1 & \frac{T_2}{\sqrt{2}} \\ 0 & 0 & -T_1 & -\frac{T_2}{\sqrt{2}} \\ T_1 & -T_1 & 0 & 0 \\ \frac{T_2}{\sqrt{2}} & -\frac{T_2}{\sqrt{2}} & 0 & 0 \end{pmatrix}, \quad (16)$$

where

$$T_1 = \frac{m_t}{\sqrt{s}} [(\kappa_L^{CC})^2 + 2\kappa_L^{CC} + (\kappa_R^{CC})^2], \quad (17)$$

$$T_2 = \frac{m_t}{\sqrt{s}} [(1 + \kappa_L^{NC} - \kappa_R^{NC})^2 - 1], \quad (18)$$

and we have retained only the terms which grow with s . For the color singlet $J = 1$ partial wave, the coupled channel matrix for the channels $t_+\bar{t}_+$, $t_+\bar{t}_-$, $t_-\bar{t}_+$, $t_-\bar{t}_-$, and $W_L^+W_L^-$ is

$$a^1 = \frac{\sqrt{6}G_F}{48\pi}s \begin{pmatrix} 0 & 0 & 0 & 0 & T_3 \\ 0 & 0 & 0 & 0 & -\sqrt{2}T_4 \\ 0 & 0 & 0 & 0 & -\sqrt{2}T_5 \\ 0 & 0 & 0 & 0 & -T_3 \\ T_3 & -\sqrt{2}T_4 & -\sqrt{2}T_5 & -T_3 & 0 \end{pmatrix}, \quad (19)$$

where

$$T_3 = \frac{m_t}{\sqrt{s}} [(\kappa_L^{CC})^2 + 2\kappa_L^{CC} + (\kappa_R^{CC})^2 - \kappa_L^{NC} - \kappa_R^{NC}], \quad (20)$$

$$T_4 = (\kappa_R^{CC})^2 - \kappa_R^{NC}, \quad (21)$$

$$T_5 = (\kappa_L^{CC})^2 + 2\kappa_L^{CC} - \kappa_L^{NC}, \quad (22)$$

and again we have retained only the terms which grow with s .

The characteristic equations for the roots of Eqs. 16 and 19 are easily found. The strongest constraint in each case comes from the largest eigenvalue,

$$a_{max}^0 = \frac{\sqrt{6}G_F s}{16\pi} \sqrt{2T_1^2 + T_2^2}, \quad (23)$$

for $J = 0$ and

$$a_{max}^1 = \frac{\sqrt{6}G_F s}{48\pi} \sqrt{2[T_3^2 + T_4^2 + T_5^2]}, \quad (24)$$

for $J = 1$, where partial-wave unitarity requires $a_{max}^J < 1$. Although the importance of the higher partial waves are generally reduced by an overall factor $2J + 1$, since some of the $J = 1$ amplitudes grow linearly with s and the $J = 0$ amplitudes grow only as $m_t\sqrt{s}$, the $J = 1$ amplitudes give the most significant constraints for the processes we are considering. Constraints on the parameters from these bounds are shown in Figs. 3a and 3b for κ_L^{NC} versus κ_R^{NC} and κ_L^{CC} versus κ_L^{NC} , respectively, for different values of the scale \sqrt{s} where unitarity is saturated, where the other parameters are set to zero in each case. The regions allowed by precision electroweak data are taken from the corresponding cases in Fig. 1.

If we assume that partial-wave unitarity is obeyed up to the energy scale of new physics, then the unitarity bounds in Fig. 3 for a given value of \sqrt{s} can be interpreted as the limits on the anomalous couplings when the new physics scale is equal to that value of \sqrt{s} . The scale at which unitarity constraints begin to encroach on the region allowed by the LEP and SLC data varies according to the parameter set used. The lowest energy scales for which the unitarity constraints place additional limits on the new physics parameters (\sqrt{s}_{min}) are listed in the first column of Table I for various parameter sets.

As the new physics scale is increased, the region allowed by unitarity shrinks towards the Standard Model point (where all the κ 's are zero). The allowed regions in Figs. 1 and 2 (determined by the precision electroweak data) do not include the Standard Model (as expected from the $\delta_{b\bar{b}}$ measurement), and predict nonzero values for the κ parameters. There is then a maximum value of \sqrt{s} (\sqrt{s}_{max}) for which both the unitarity and precision electroweak

constraints are satisfied. The quantity \sqrt{s}_{max} can be interpreted as an approximate upper bound on the scale of the new physics which is embodied in the anomalous interactions of Eq. 1. Values of \sqrt{s}_{max} for various parameter sets are given in second column of Table I when the 90% CL LEP and SLC data are used.

When we tighten the LEP and SLC constraints by requiring 68% CL agreement with the data, only κ_R^{NC} versus κ_L^{CC} has a region of values consistent with the data when only two parameters are allowed to vary. Figure 4 shows this allowed region and the unitarity constraints for various values of \sqrt{s} . The maximum value of \sqrt{s} for which both unitarity and the electroweak constraints are satisfied is $\sqrt{s}_{max} = 3.6$ TeV for $\mu = 2m_t$. When the full three-parameter set is considered, this increases slightly to

$$\sqrt{s}_{max} = 3.7 \text{ TeV}, \quad \kappa_R^{NC}, \kappa_L^{NC}, \kappa_L^{CC} \neq 0. \quad (25)$$

We have also examined the effect on our results of changing the renormalization scale μ . Since each of the electroweak observables in Eqs. 2-5 are proportional to $\log(\mu^2/M_Z^2)$, reducing μ to m_t will shift the allowed regions in Figs. 1 and 2 to larger values of the couplings, which in turn leads to smaller values of \sqrt{s}_{min} and \sqrt{s}_{max} (see Table I). On the other hand, if $\mu > 2m_t$ is chosen, then the allowed regions shrink in size; however, such larger values of the renormalization scale μ are not physically reasonable. Therefore, the energy scales listed in Table I and Eq. 25 for $\mu = 2m_t$ represent conservative estimates. Choosing a renormalization scale as low as m_t typically reduces these values by 30%.

In summary, our analysis shows that unitarity constraints can impose limits on the anomalous weak gauge couplings of the top quark beyond those given by precision electroweak data if the new physics responsible for these couplings appears at a scale Λ as low as 2 TeV, as indicated by the values of \sqrt{s}_{min} in Table I. Furthermore, if the deviation from the standard model in the precision electroweak measurements is due to such couplings, then there is a 68% CL upper bound on Λ of 3.7 TeV.

I. ACKNOWLEDGEMENTS

We thank Xinmin Zhang for many helpful discussions. This work was supported in part by the U.S. Department of Energy under Contract DE-FG02-94ER40817. M. Hosch was also supported under a GAANN fellowship.

REFERENCES

- [1] CDF Collaboration, F. Abe *et al.*, Phys. Rev. Lett. **74**, 2626 (1995).
- [2] D0 Collaboration, S. Abachi *et al.*, Phys. Rev. Lett. **74**, 2632 (1995).
- [3] K. Mönig, talk presented at *ICHEP-96*, Warsaw, Poland, September, 1996.
- [4] R. Peccei and X. Zhang, Nucl. Phys. **B337**, 269 (1990); R. Peccei, S. Peris, and X. Zhang, Nucl. Phys. **B349**, 305 (1991); B.-L. Young and X. Zhang, Phys. Rev. **D51**, 6584 (1995).
- [5] G.J. Gounaris, M. Kuroda, and F.M. Renard, preprint PM/96-22 and THES-TP 96/06, hep-ph/9606435, June 1996; G.J. Gounaris, F.M. Renard, and C. Verzegnassi, Phys. Rev. **D52**, 451 (1995), and references therein.
- [6] S. Dawson and G. Valencia, Phys. Rev. **D53**, 1721 (1996); E. Malkawi and C.P. Yuan, Phys. Rev. **D50**, 4462 (1994).
- [7] T.D. Lee and C.N. Yang, Phys. Rev. Lett. **4**, 307 (1960); B. Lee, C. Quigg, and H. Thacker, Phys. Rev. **D16**, 1519 (1977); T. Appelquist and M.S. Chanowitz, Phys. Rev. Lett. **59**, 2405 (1987).
- [8] K. Whisnant, B.-L. Young, and X. Zhang, Phys. Rev. **D52**, 3115 (1995).
- [9] G.J. Gounaris, D.T. Papadamou, and F.M. Renard, preprint PM/96-28 and THES-TP 96/09, hep-ph/9609437, September, 1996.
- [10] P. Langacker, talk presented at *SUSY-95*, Palaiseau, France, May, 1995, U. of Penn report UPR-0683T.
- [11] D.C. Kennedy and B.W. Lynn, Nucl. Phys. **B322**, 1 (1989); M. Peskin and T. Takeuchi, Phys. Rev. Lett. **65**, 964 (1990); Phys. Rev. **D46**, 381 (1992); G. Altarelli, R. Barbieri, and F. Caravaglios, Nucl. Phys. **B405**, 3 (1993).
- [12] G. Altarelli, R. Barbieri, and F. Caravaglios, Nucl. Phys. **B363**, 326 (1991).
- [13] M. Alam *et al.*, CLEO collaboration, Phys. Rev. Lett. **74**, 2885 (1995).
- [14] K. Fujikawa and A. Yamada, Phys. Rev. **D49**, 5890 (1994).
- [15] M.S. Chanowitz, M.A. Furman, and I. Hinchliffe, Nucl. Phys. **B153**, 402 (1979).

TABLES

TABLE I. Values of \sqrt{s}_{min} (the lowest energy scale for which unitarity places additional limits on the anomalous parameters) and \sqrt{s}_{max} (the highest energy scale for which both the unitarity and electroweak constraints are satisfied) at 90% CL for various parameter sets when $\mu = 2m_t$. The corresponding values for $\mu = m_t$ are given in parentheses.

Nonzero parameters	\sqrt{s}_{min} (TeV)	\sqrt{s}_{max} (TeV)
$\kappa_L^{NC}, \kappa_R^{NC}$	3.4 (2.6)	19 (13)
$\kappa_L^{NC}, \kappa_L^{CC}$	3.3 (2.1)	13 (9)
$\kappa_R^{NC}, \kappa_L^{CC}$	1.9 (1.3)	19 (13)
$\kappa_L^{NC}, \kappa_R^{NC}, \kappa_L^{CC}$	1.6 (1.3)	20 (14)

FIGURE CAPTIONS

FIG. 1. Limits from precision LEP and SLC data on (a) κ_R^{NC} vs. κ_L^{NC} for $\kappa_L^{CC} = \kappa_R^{CC} = 0$, and (b) κ_L^{CC} vs. κ_L^{NC} for $\kappa_R^{NC} = \kappa_R^{CC} = 0$, using the 90% CL limits on S , T and U from Ref. [10], and on $\delta_{b\bar{b}}$ from Ref. [3]. The regions allowed by the electroweak variables S , T , U and $\delta_{b\bar{b}}$ are indicated by the arrows. In Fig. 1(a) the entire region shown is allowed by U . In each case the region allowed by all of the electroweak data lies inside the bold lines.

FIG. 2. Allowed region from precision LEP and SLC data of κ_L^{NC} vs. κ_R^{NC} for several values of κ_L^{CC} with $\kappa_R^{CC} = 0$, using the 90% CL limits from Refs. [3] and [10].

FIG. 3. Unitarity limits on (a) κ_R^{NC} vs. κ_L^{NC} for $\kappa_L^{CC} = \kappa_R^{CC} = 0$, and (b) κ_L^{CC} vs. κ_L^{NC} for $\kappa_R^{NC} = \kappa_R^{CC} = 0$, shown for several values of \sqrt{s} . The regions allowed by unitarity lie inside the circles in (a), and between the lines for each energy scale in (b). The 90% CL regions allowed by LEP and SLC data, taken from Fig. 1, are also shown.

FIG. 4. Unitarity limits on κ_R^{NC} vs. κ_L^{CC} for $\kappa_L^{NC} = \kappa_R^{CC} = 0$, shown for several values of \sqrt{s} . The regions allowed by unitarity lie inside the ellipses for each energy scale. The 68% CL region allowed by LEP and SLC data is also shown.

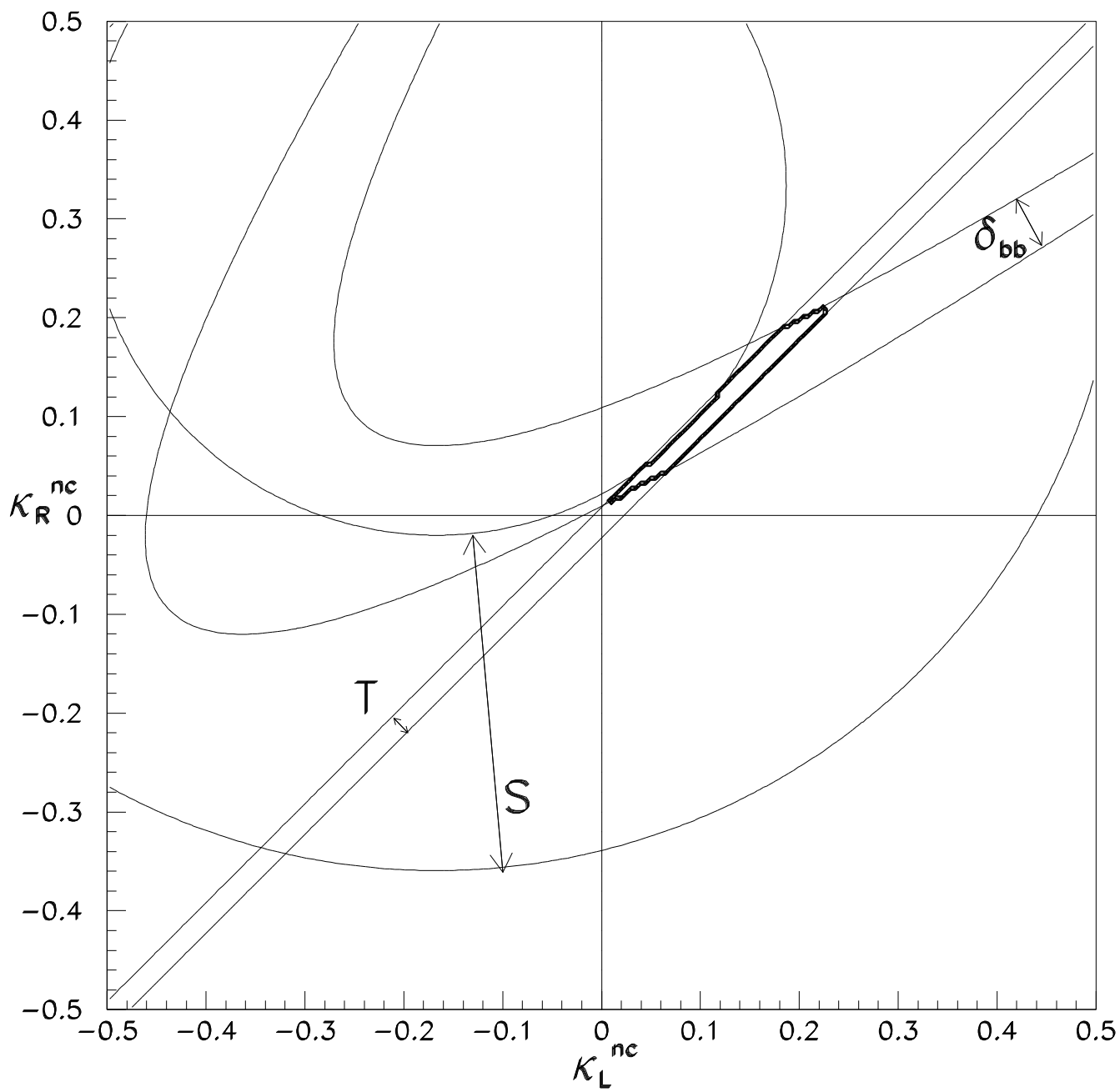


fig. 1(a)

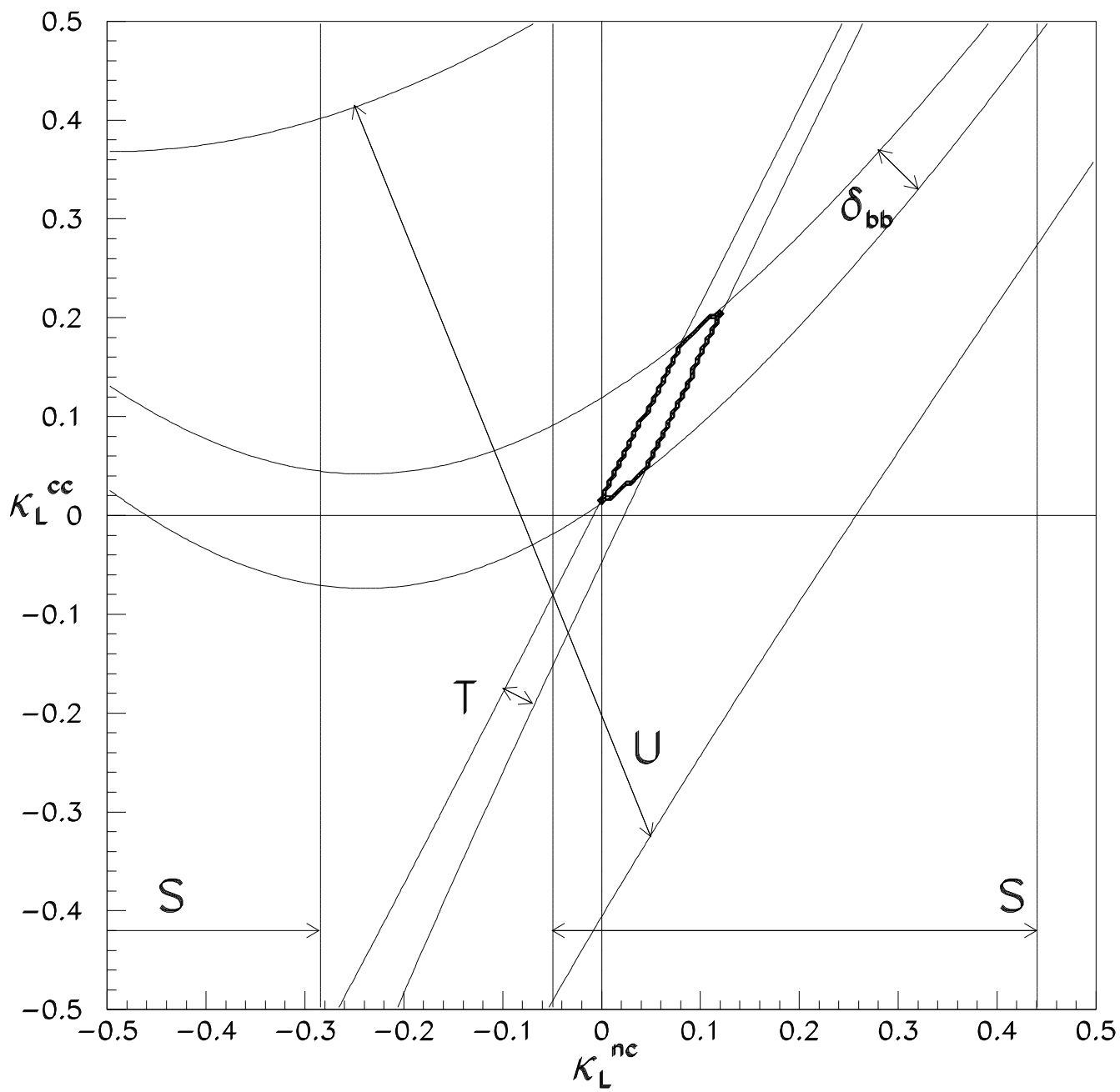


fig. 1(b)

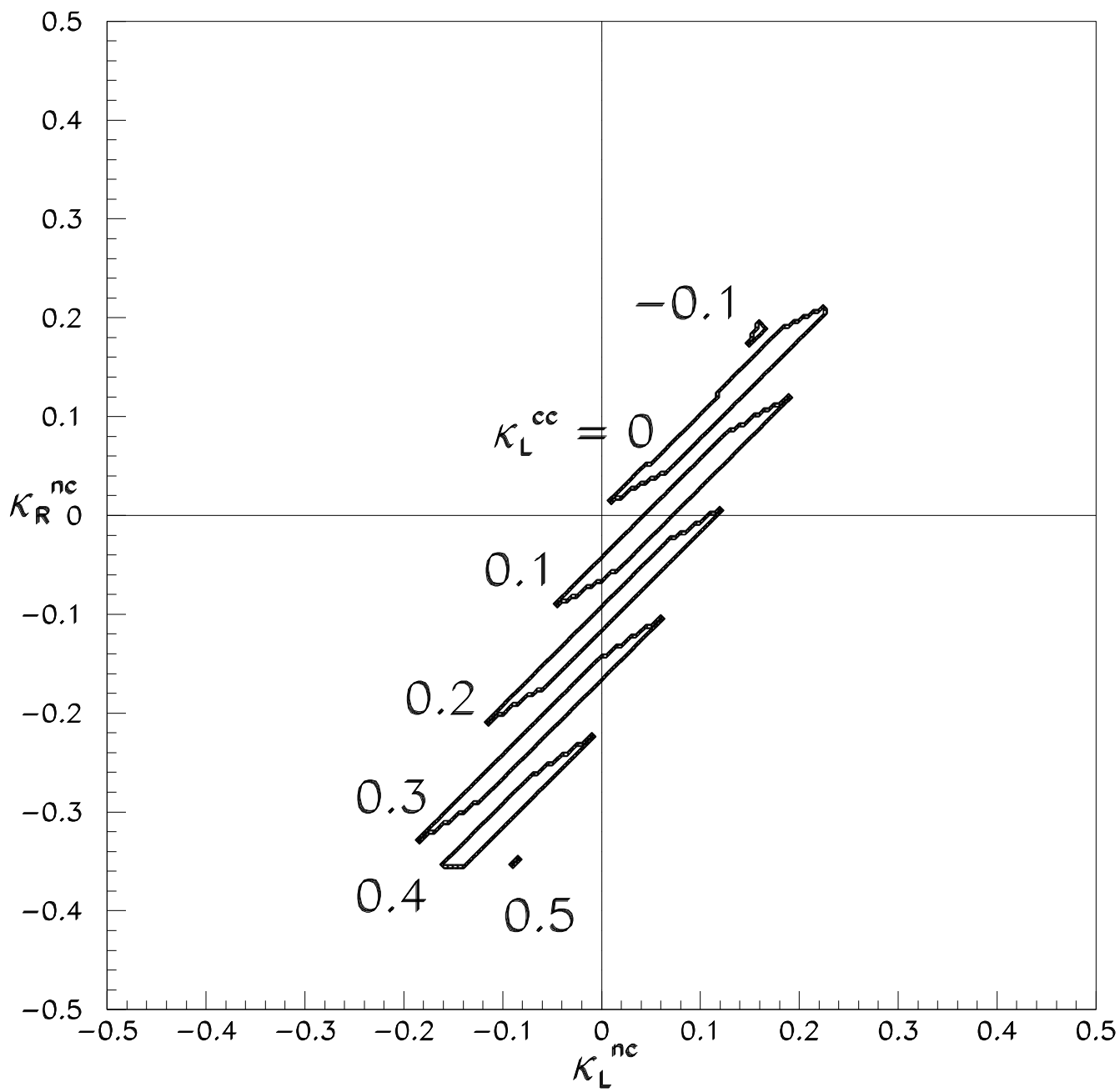


fig. 2

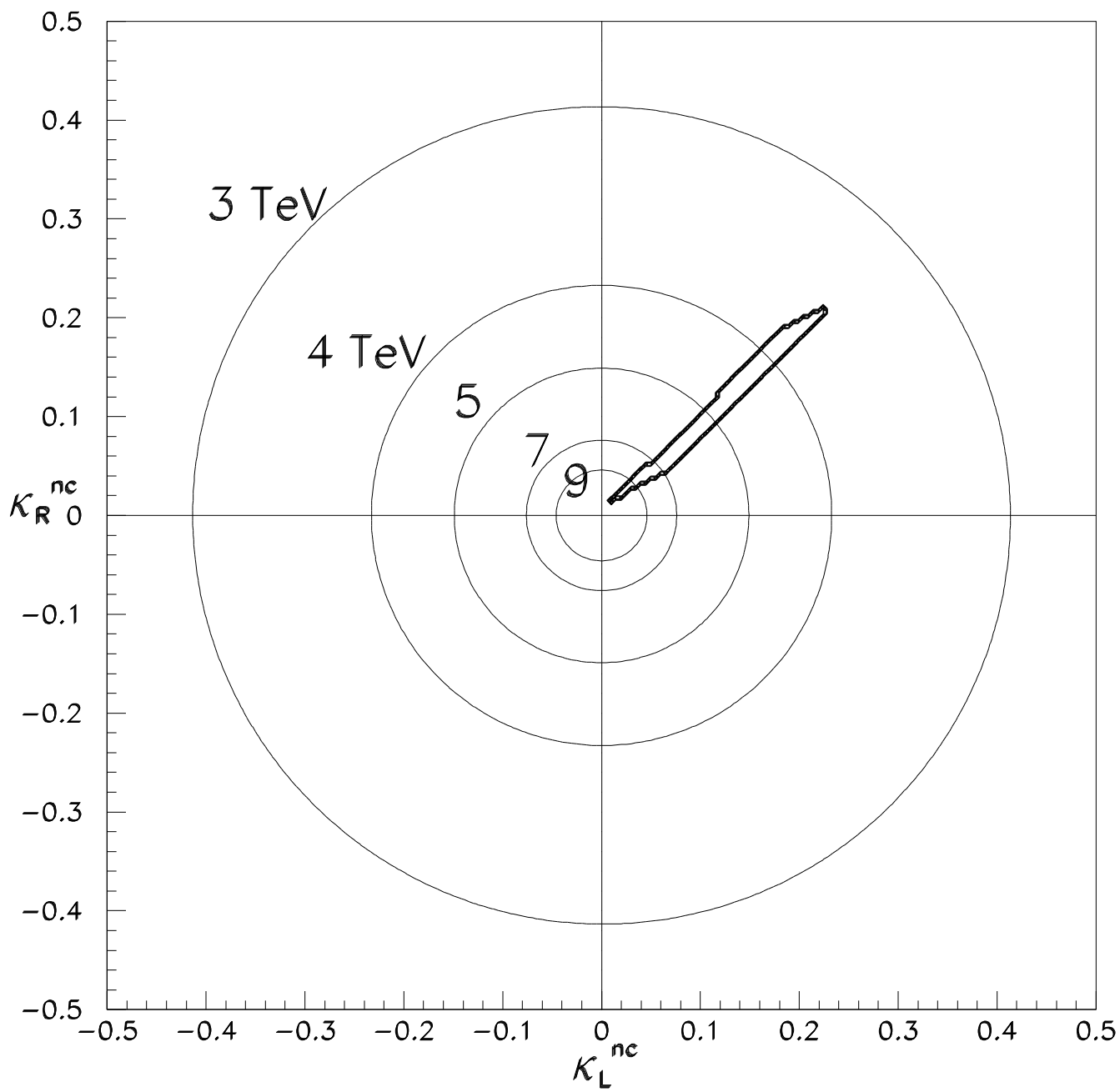


fig. 3(a)

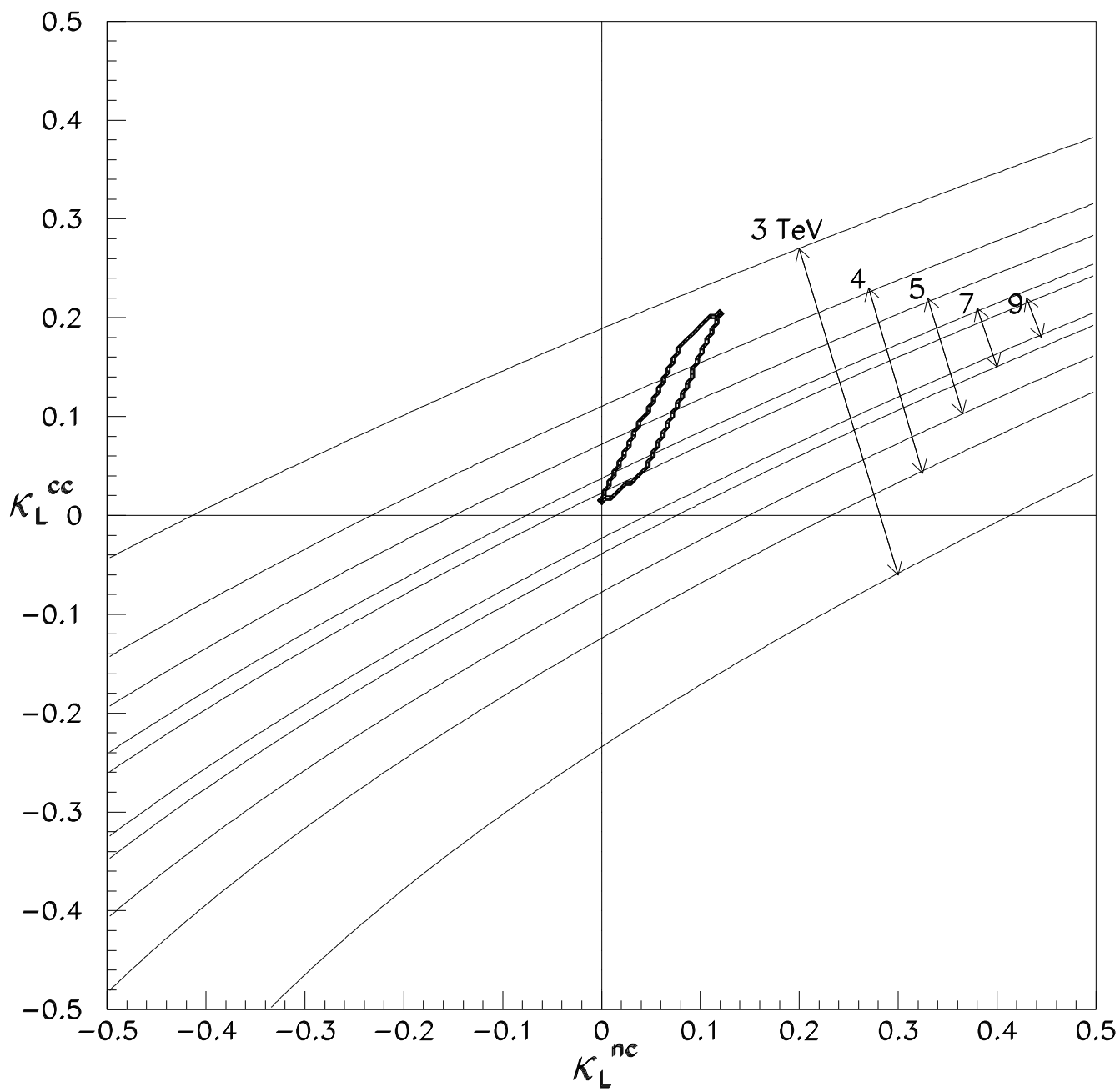


fig. 3(b)

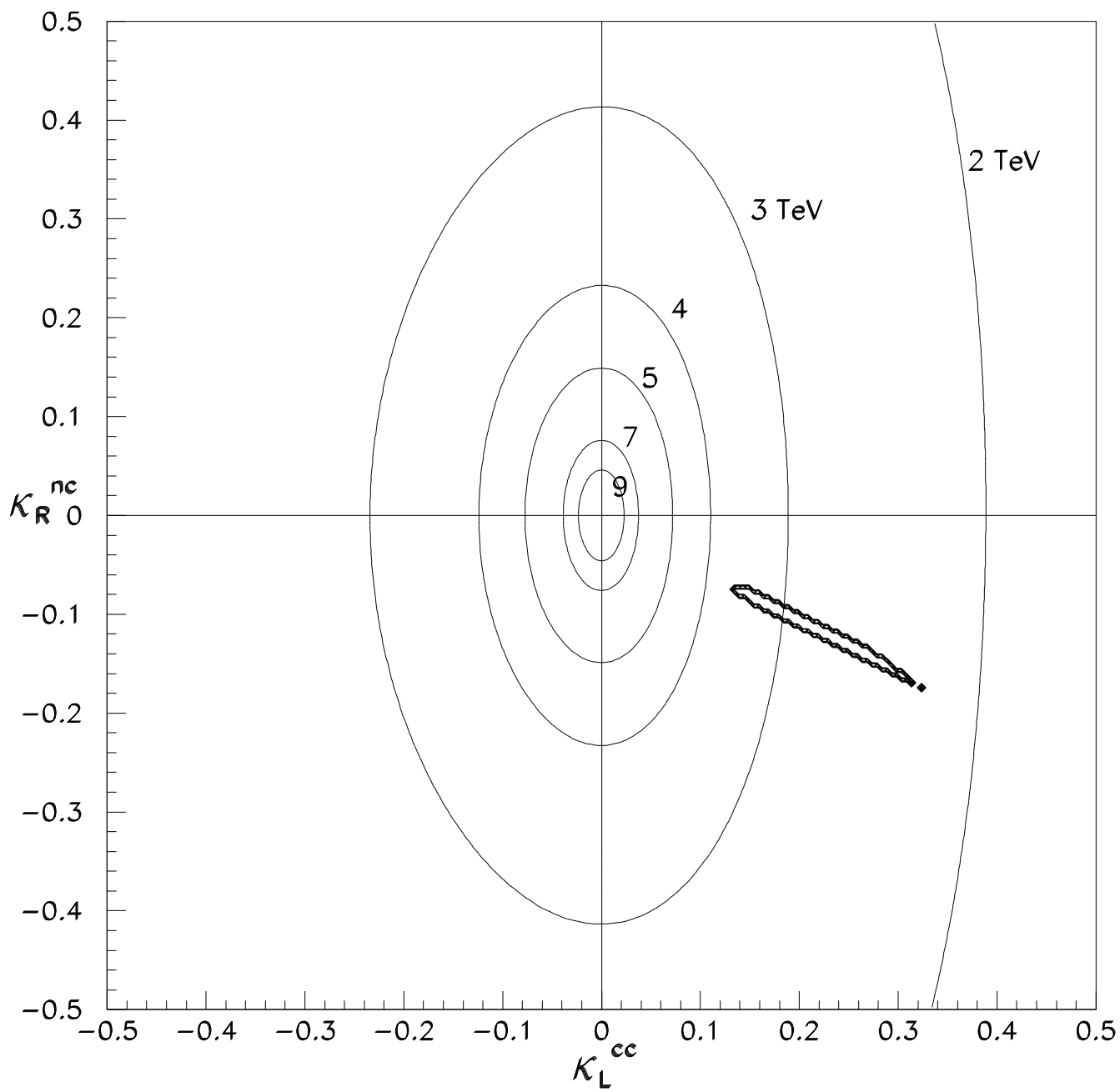


fig. 4